Diagn Interv Radiol 2024; DOI: 10.4274/dir.2024.242975

NEURORADIOLOGY

ORIGINAL ARTICLE

The value of dual-energy computed tomography angiography-based virtual monoenergetic imaging for evaluations after cerebral aneurysm clipping

Zhihua Lu[1]
Suying Wu[1]
Feijian Wu[1]
Qingdong Jin[2]
Qingjing Huang[1]
Baoteng Zhang[1]

[1]The First Hospital of Putian City, Department of Radiology, Putian, China

[2]The First Hospital of Putian City, Department of Neurosurgery, Putian, China

PURPOSE

This study aimed to research the optimal energy range of dual-energy computed tomography angiography (DECTA)-based virtual monoenergetic imaging (VMI) for evaluations after cerebral aneurysm clipping.

METHODS

Sixty patients who underwent DECTA after cerebral aneurysm clipping were analyzed retrospectively. Conventional computed tomography angiography (CTA) was compared with VMIs at 60, 70, 80, 90, and 100 keV. The mean attenuation and standard deviation values within the regions of interest placed in the brain parenchyma and arteries with the worst artifact were measured, respectively. The ΔCT and artifact index (AI) values were calculated to assess the artifact severity. The contrast-to-noise ratio (CNR) was calculated to assess vascular contrast. Two radiologists assessed brain parenchyma and cerebrovascular scores qualitatively using a five-point Likert scale.

RESULTS

Quantitative analysis showed that the artifacts of VMIs were significantly reduced compared with conventional CTA ($P \leq 0.014$), except for the ΔCT and AI of 60 keV and the ΔCT of 70 keV. However, there was no significant difference in the vascular contrast on VMIs compared with conventional CTA, except for the CNR of 60 keV ($P = 0.008$). In qualitative analysis, the proportions of brain parenchyma scores and cerebrovascular scores ≥4 on the VMIs of 70 and 80 keV were higher than those of conventional CTA and other VMIs.

CONCLUSION

For the patients who underwent DECTA after cerebral aneurysm clipping, the 70–80 keV VMIs are expected to be the optimal energy range for balancing clip artifacts and visibility of adjacent vessels.

CLINICAL SIGNIFICANCE

Studying the optimal energy range of DECTA-based VMI for post-operative assessment of aneurysm clipping can reduce metal artifacts in images and increase vascular contrast. This facilitates the follow-up of patients after aneurysm clipping, offers timely and accurate detection of postoperative complications, provides assistance to clinicians in diagnosis and treatment, and improves patient prognosis.

KEYWORDS

Dual-energy, computed tomography angiography, virtual monoenergetic imaging, aneurysm clipping, metal artifact

Corresponding author: Baoteng Zhang

E-mail: 519145686@qq.com

Received 14 August 2024; revision requested 09 September 2024; accepted 29 October 2024.

Epub: 16.12.2024

Publication date:

DOI: 10.4274/dir.2024.242975

You may cite this article as: Lu Z, Wu S, Wu F, Jin Q, Huang Q, Zhang B. The value of dual-energy computed tomography angiography-based virtual monoenergetic imaging for evaluations after cerebral aneurysm clipping. *Diagn Interv Radiol.* 16 December 2024 DOI: 10.4274/dir.2024.242975 [Epub Ahead of Print].

Cerebral aneurysms are localized weakened pouches formed by pathological rupture of the internal elastic lamina and media of the arterial wall.[1] The incidence of unruptured cerebral aneurysms in the general population is 3.6%–6%,[2] and they are mostly asymptomatic or have non-specific symptoms. Ruptured cerebral aneurysms are a neurosurgical emergency with potentially devastating consequences, which may be accompanied by complications, such as subarachnoid hemorrhage, hydrocephalus, cerebral parenchymal hemorrhage, and epidural hematoma.[2] Surgical clipping can safely treat ruptured and unruptured cerebral aneurysms.[3] However, there are still risks, such as incomplete clipping, residue or recurrence of the aneurysm, distal occlusion of the parent artery, cerebral vasospasm, and cerebral hemorrhage.[4-6] As a non-invasive and simple technique, computed tomography angiography (CTA) is widely used to evaluate treated aneurysms. Early postoperative evaluation helps identify complications in time and serves as a basis for late follow-up.[7] However, surgically implanted clips produce metal artifacts, affecting the observation of fine structures, such as peripheral brain parenchyma and vessels. Therefore, it is essential to minimize metal artifacts.

In recent years, several studies have applied different techniques to reduce metal artifacts in patients with treated cerebral aneurysms, among which metal artifact reduction (MAR) algorithms and dual-energy computed tomography angiography (DECTA)-based virtual monoenergetic imaging (VMI) can effectively improve image quality and reduce metal artifacts.[8-12] Low-keV monoenergetic images can improve density resolution and enhance the contrast between vessels and brain parenchyma; however, the noise and metal artifacts are worsened. In contrast, high-keV monoenergetic images can reduce metal artifacts, but the contrast is also reduced. Therefore, finding the optimal energy range to balance clip artifacts and visibility of adjacent vessels is crucial. To our knowledge, there are very few studies to address this issue.[10-12] For instance, a skull phantom study[10] showed that 120keV VMI significantly reduced metal artifacts and improved visibility of adjacent vessels compared with non-corrected DECTA, but they did not study the value of other energy levels. Furthermore, Dunet et al.[11] demonstrated the best compromise between MAR and relative contrast-to-noise ratio (CNR) was obtained at 70–75 keV for gemstone spectral imaging (GSI) DECTA after cerebral aneurysm clipping. However, their results were not compared with conventional CTA.

Main points

- Metal artifacts on the tail of the clip were more serious than those on the head on both conventional computed tomography angiography (CTA) and virtual monoenergetic imaging (VMI).
- VMI can significantly reduce metal artifacts compared with conventional CTA, except for 60 keV.
- Metal artifacts of clips near the skull base were higher than those away from the skull base on both conventional CTA and VMIs.
- The 70–80 keV VMIs are expected to be the optimal energy range for balancing clip artifacts and visibility of adjacent arteries.

In the current study, we comprehensively evaluate the effects of artifacts in the head, tail, and middle part of the implanted clip on peripheral vessels and brain parenchyma by comparing VMIs with conventional CTA to find the optimal energy range of DECTA-based VMI for evaluation after cerebral aneurysm clipping.

Methods

Population and design

One hundred twelve patients who underwent aneurysm surgical clipping in the First Hospital of Putian City between March 2019 and July 2023 were collected. The inclusion criteria were as follows: (1) early follow-up DECTA performed after surgical clipping (the interval between examination and operation was <4 weeks); (2) no pregnancy, no history of iodine contrast allergy, and no severe cardiopulmonary and renal dysfunction. The exclusion criteria were as follows: (1) different scanners and different concentrations of contrast media; (2) poor image quality or incomplete clinical data; (3) multiple aneurysms or use of multiple metal clips. Figure 1 shows the flowchart of inclusion and exclusion criteria for the study. This retrospective study was approved by the First Hospital of Putian City Hospital Ethics Committee on December 28, 2022 (protocol no: 2022-100), and patient written consent was waived.

Image acquisition and reconstruction

All patients underwent DECTA on a third-generation dual-source computed tomography (CT) scanner (SOMATOM Force, Siemens Medical Solutions, Forchheim, Germany). The patients were in the supine position. The scanning range was from the 1 cm level below the skull base to the top of the skull, from foot to head. Scanning parameters were as follows: tube voltages 80 kVp and 150 kVp, pitch 0.7 mm, field of view 200 × 200 mm. Automated tube current modulation (CareDose4D, Siemens Medical Solutions) was adopted. Reconstruction parameters were as follows: Matrix 512 × 512, layer thickness 1.0 mm, spacing 0.7 mm, convolution kernel Qr40.

Ultravist (370 mg/mL; Bayer-Schering Healthcare, Berlin, Germany) was injected into the anterior cubital vein with a double-barrel high-pressure syringe at a dose of 1.0 mL/kg and rate of 4.5 mL/s, followed by a 40 mL saline flush at the same rate. The acquisition was started automatically 4 seconds after the peak time when the attenuation value of the ascending aorta reached 100 HU.

After the scanning, the automatically reconstructed 80 kV, Sn150 kV, and blended 115 kV images were transmitted to a Siemens workstation (Syngo.via VB10B) for post-processing. The Monoenergetic module was used to reconstruct the VMIs every 10 keV from 60 to 100 keV. The blended 115 kV image using a ratio of 50/50 from the 80 kV and Sn150 kV data is approximately equivalent to a conventional 120 kV acquisition and was considered as the reference. Finally, six groups of images were obtained for subsequent analysis.

Objective evaluation of image quality

Selection of regions of interest

Objective image analysis was performed by a board-certified neuroradiologist with 11 years of experience in brain imaging. A 10 mm^2 circular region of interest (ROI) was placed within the center of one occipital lobe parenchyma (OLP) as the reference OLP, avoiding vessels, calcification, malacic foci, and hemorrhage.[13] Another ROI (as large as possible) was placed in the basilar artery as the reference BA, avoiding vascular wall calcification and skull base artifacts. Regions of interest A, B, and C between 6 and 8 mm^2 (mean 7.2 mm^2) were placed in the brain parenchyma, with the worst artifacts around the head, tail, and middle part of the implanted clip, respectively. Regions of interest D and E were placed in the vessels with the worst artifacts around the head/tail and middle part of the implanted clip, respectively. These ROIs were copied in the same locations on both conventional CTA and VMIs (Figure 2). These ROIs' attenuation

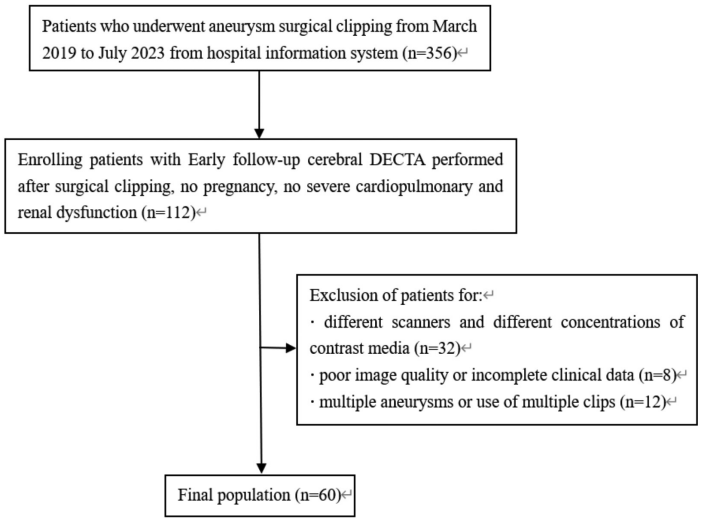

Figure 1. The flowchart of inclusion and exclusion criteria for the study. DECTA, dual-energy computed tomography angiography.

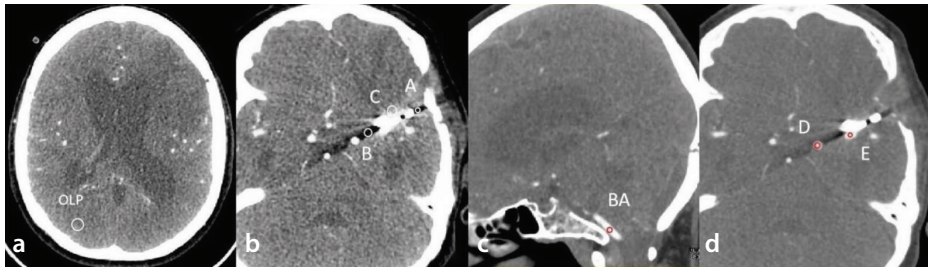

Figure 2. An example of manually designating regions of interest in conventional computed tomography angiography images at different slices or different window widths and levels. **(a)** The occipital lobe parenchyma is drawn in the right occipital lobe, avoiding vessels, malacic foci, and hemorrhage. **(b)** Draw A, B, and C in the areas with the worst artifacts in the metal clip's head, tail, and middle part, respectively. **(c)** BA is located in the basilar artery. **(d)** D and E are located in the vessels with the worst artifacts in the tail and middle part of the metal clip, respectively.

and standard deviation (SD) values were recorded. Each ROI was measured three times to calculate the average value for further analysis. In addition, images of 30 patients were randomly selected, and the ROIs were measured by another well-trained neurosurgeon in a blinded method to assess the inter-reader agreement.

Quantitative analysis

The ΔCT values between A, B, C, and OLP and between D, E, and BA were calculated using the following formula:

$$\Delta CT = |\, CT_{artifact} - CT_{reference} \,| \quad (1).$$

The artifact index (AI) values of A, B, C, D, and E and the CNR values of D and E were calculated using the following formula[9]:

$$AI = \sqrt{SD^2_{artifact} - SD^2_{reference}} \quad (2)$$

$$CNR = \frac{|CT_{artifact} - CT_{reference}|}{\sqrt{\left(SD^2_{artifact} - SD^2_{reference}\right)/2}} \quad (3)$$

Artifact severity was assessed quantitatively by ΔCT (1) and AI (2). Vascular contrast was assessed quantitatively by CNR (3).

Subjective evaluation of image quality

A five-point Likert scale[8] was used to evaluate the artifact severity of brain parenchyma and the contrast of adjacent arteries subjectively (Supplementary Table S1). Subjective image analysis was carried out independently by two more well-trained radiologists 1 and 2.

Statistical analysis

The statistical analysis was performed using SPSS statistics version 25.0 (IBM, Chicago, Illinois, USA). For the quantitative analysis, inter-reader and intra-reader agreements regarding attenuation and SD values of ROIs were calculated using intraclass correlation coefficients (ICCs). All ICCs between 0.75 and 1.00 were interpreted as excellent agreement. A comparison of data from the six groups of images was performed by one-way analysis of variance (ANOVA). According to the homogeneity of variance, the least significant difference or Tamhane's T2 test was used to compare ΔCT, AI, and CNR between conventional CTA and VMIs. A graphical comparison was used to illustrate the results. In addition, to evaluate whether the clips' location may affect the metal artifact severity of conventional CTA and VMIs, as previously suggested,[11] ΔCT and AI were also compared between patients with clips near the skull base (internal carotid artery or communicating arteries) and patients with clips away from the skull base (anterior cerebral artery, middle cerebral artery, or posterior cerebral artery) in the six groups of images using the Mann–Whitney U test. To avoid the influence of different orientations of clips, the worst ΔCT and AI values from ROI A, B, and C were selected for artifact severity comparison.

For the qualitative analysis, the inter-reader agreement of subjective scores (brain parenchyma scores and cerebrovascular scores) were calculated using Cohen's kappa coefficients, with values of 0.41–0.60 representing a moderate agreement, 0.61–0.80 a strong agreement, and 0.81–1.00 an almost perfect agreement. Every disagreement was resolved by consensus between two radiologists before further analysis. The chi-squared test was used to compare subjective scores ≥4 proportions between conventional CTA and VMIs. A *P* value of <0.05 was considered statistically significant.

Results

Finally, 60 patients (of whom the mean age was 55.15 ± 9.24 years and 23 were men) underwent surgical clipping, and 60 aneurysms were included in this study (one metal clip per aneurysm). In summary, seven different clips (Yasargil, Braun Medical, Tuttlingen, Germany) made of titanium were included, and the blade length was 7.0–13.7 mm (Supplementary Table S2). The dose-length product (DLP) was 158.00 ± 31.45 mGy·cm, the computed tomography dose index (CTDIvol) was 8.75 ± 1.74 mGy, and the effective dose (ED) was 0.33 ± 0.07 mSv according to ICRP 103 conversion coefficients.[13] The radiation dose in the current study is lower than that in previous cerebral DECTA-related studies (DLP: 280–685 mGy·cm, CTDIvol: 13–42 mGy, ED: 0.59–1.44 mSv).[11,12,14,15] The interval be-

tween postoperative DECTA and surgery was 16.77 ± 5.64 days. Supplementary Table S3 summarizes patient characteristics as well as aneurysm location and postoperative complications.

Quantitative analysis

The inter-reader and intra-reader ICCs of attenuation and SD values in conventional CTA and VMIs are summarized in Supplementary Table S4. All ICCs showed excellent agreement (inter-reader ICCs: 0.892–0.985, intra-reader ICCs: 0.911–0.995). The ΔCT_A, ΔCT_B, ΔCT_C, AI_A, AI_B, and AI_C of the brain parenchyma and the ΔCT_D, ΔCT_E, AI_D, AI_E, CNR_D, and CNR_E of the cerebral vessels were all in concordance with the normal or slightly skew distribution. The *P* values of one-way ANOVA were all <0.05, except for CNR_D. There were significant differences for ΔCT_A, ΔCT_B, and ΔCT_C of all VMIs compared with those of conventional CTA ($P \leq 0.002$). They were all lower as the keV level increased, and the lowest values were 44.39 ± 24.40, 60.97 ± 34.42, and 30.28 ± 10.91, respectively, at 100 keV (Table 1, Figure 3a). Except for 60 keV, there were significant differences for AI_A, AI_B, and AI_C of all VMIs compared with those of conventional CTA ($P \leq 0.014$). They were all lower as the keV level increased, and the lowest values were 17.83 ± 10.50, 23.93 ± 16.90, and 15.92 ± 5.81, respectively (Table 2, Figure 3b). The ΔCT and AI of clips near the skull base were higher than those of clips away from the skull base on both conventional CTA and VMIs, with significant differences ($P \leq 0.031$), except for the AI of 90 and 100 keV (Supplementary Table S5).

Except for ΔCT_D and ΔCT_E of 60 keV and ΔCT_E of 70 keV, the ΔCT_D and ΔCT_E of all VMIs were significantly different from those of conventional CTA ($P \leq 0.003$). They basically decreased with the increase in keV level, and the lowest values were 28.47 ± 17.72 and 51.63 ± 28.55, respectively (Table 3, Figure 4a). The AI_D and AI_E of all VMIs differed significantly from those of conventional CTA ($P < 0.001$). They all decreased with the increase in keV level, and the lowest values were 21.20 ± 6.05 and 29.88 ± 12.14, respectively (Table 4, Figure 4b). However, there was no significant difference in CNR_D and CNR_E between all VMIs and conventional CTA, except for the CNR_E of 60 keV ($P = 0.008$) (Table 4, Figure 4c).

Qualitative analysis

The Cohen's kappa coefficients of brain parenchyma and cerebrovascular scores of radiologists 1 and 2 in conventional CTA and VMIs are summarized in Supplementary Table S6. All kappa coefficients showed strong or almost perfect agreement (0.633–0.832). In conventional CTA and 60 to 100 keV VMIs, the proportions of brain parenchyma scores ≥4 were 6.67%, 6.67%, 61.67%, 80.00%, 20.00%, and 5.00%, respectively. Except for 60 and 100 keV, the brain parenchyma scores of other keV levels were significantly higher than those of conventional CTA ($P \leq 0.032$). The proportions of cerebrovascular scores ≥4 were 1.67%, 50.00%, 95.00%, 73.30%, 13.33%, and 0.00%, respectively. Except for

Table 1. ΔCT_A, ΔCT_B, and ΔCT_C in the five groups of VMIs compared with conventional CTA

Group	ΔCT_A (HU)	*P* value	ΔCT_B (HU)	*P* value	ΔCT_C (HU)	*P* value
Conventional CTA	164.95 ± 46.62	-	251.47 ± 106.01	-	101.30 ± 24.54	-
60 keV	199.18 ± 53.78	<0.001	302.41 ± 122.58	0.001	114.17 ± 28.95	0.001
70 keV	136.90 ± 38.33	<0.001	205.66 ± 83.51	0.002	79.32 ± 20.60	<0.001
80 keV	98.68 ± 32.21	<0.001	141.50 ± 59.28	<0.001	57.92 ± 17.34	<0.001
90 keV	67.11 ± 27.95	<0.001	94.86 ± 42.74	<0.001	41.17 ± 12.95	<0.001
100 keV	44.39 ± 24.40	<0.001	60.97 ± 34.42	<0.001	30.28 ± 10.91	<0.001

VMI, virtual monoenergetic imaging; CTA, computed tomography angiography; HU, hounsfield unit.

Table 2. AI_A, AI_B, and AI_C in the five groups of VMIs compared with conventional CTA

Group	AI_A (HU)	*P* value	AI_B (HU)	*P* value	AI_C (HU)	*P* value
Conventional CTA	40.89 ± 19.92	-	78.23 ± 49.72	-	34.43 ± 11.13	-
60 keV	43.85 ± 21.85	0.311	87.26 ± 57.49	0.197	37.62 ± 13.21	0.066
70 keV	31.87 ± 15.97	0.002	61.01 ± 39.38	0.014	27.65 ± 9.60	<0.001
80 keV	24.89 ± 13.20	<0.001	44.30 ± 27.42	<0.001	21.90 ± 8.24	<0.001
90 keV	20.64 ± 11.20	<0.001	31.77 ± 20.28	<0.001	18.12 ± 6.78	<0.001
100 keV	17.83 ± 10.50	<0.001	23.93 ± 16.90	<0.001	15.92 ± 5.81	<0.002

VMI, virtual monoenergetic imaging; CTA, computed tomography angiography; HU, hounsfield unit.

Table 3. ΔCT_D and ΔCT_E in the five groups of VMIs compared with conventional CTA

Group	ΔCT_D (HU)	*P* value	ΔCT_E (HU)	*P* value
Conventional CTA	94.97 ± 56.76	-	94.60 ± 53.70	-
60 keV	99.53 ± 58.61	0.681	101.42 ± 59.21	0.441
70 keV	67.44 ± 41.56	0.003	78.02 ± 44.47	0.061
80 keV	51.29 ± 33.55	<0.001	64.22 ± 35.49	0.001
90 keV	44.95 ± 72.41	<0.001	66.13 ± 60.11	0.001
100 keV	28.47 ± 17.72	<0.001	51.63 ± 28.55	<0.001

VMI, virtual monoenergetic imaging; CTA, computed tomography angiography; HU, hounsfield unit.

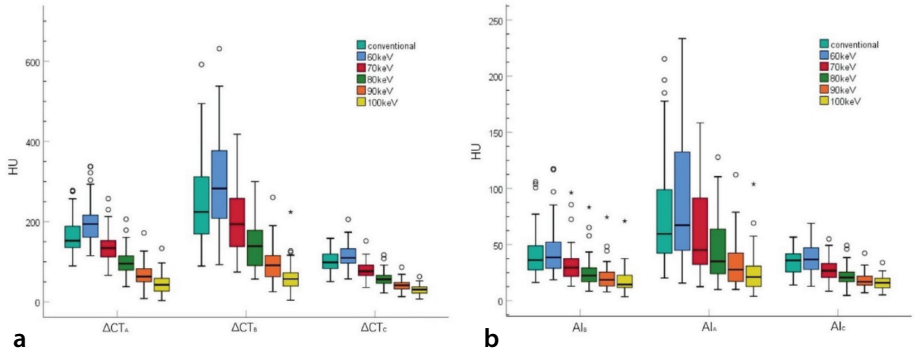

Figure 3. The box plots of the distribution of brain parenchyma parameters in conventional computed tomography angiography and virtual monoenergetic imaging with different keV levels. **(a)** The distribution of ΔCT_A, ΔCT_B, and ΔCT_C in six groups of images. **(b)** The distribution of AI_A, AI_B, and AI_C in six groups of images.

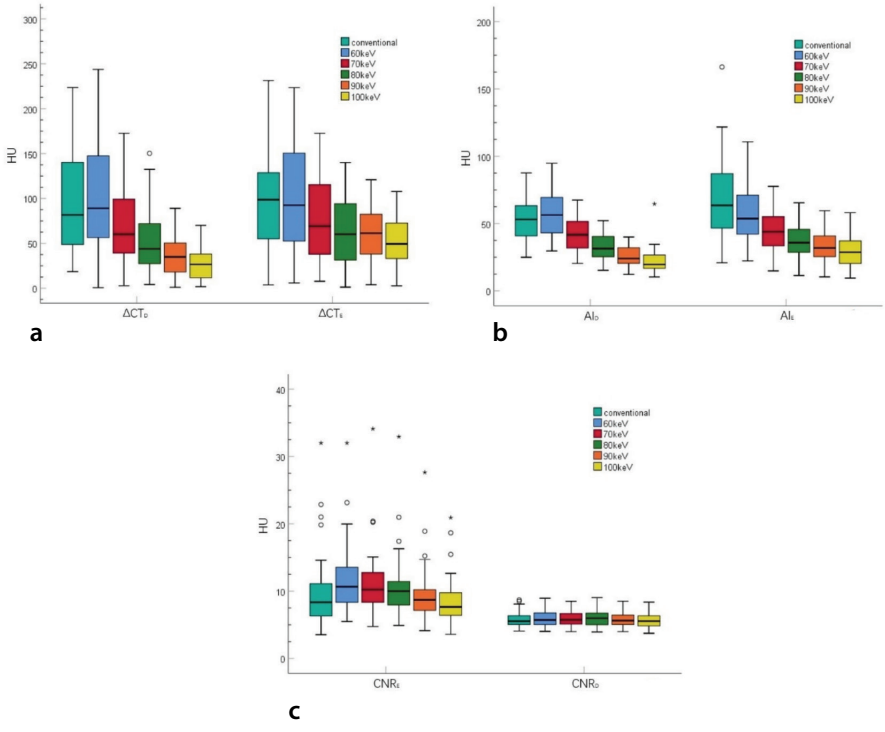

Figure 4. The box plots of the distribution of cerebrovascular parameters in conventional computed tomography angiography and virtual monoenergetic imaging with different keV levels. **(a)** The distribution of ΔCT_D and ΔCT_E in six groups of images. **(b)** The distribution of AI_D and AI_E in six groups of images. **(c)** The distribution of CNR_D and CNR_E in six groups of images.

100 keV, the cerebrovascular scores of other keV levels were significantly higher than those of conventional CTA ($P \leq 0.015$). Results are shown in Table 5. Figure 5 shows the conventional CTA and VMIs of a patient after aneurysm clipping.

Discussion

The dominant findings of our study can be summarized as follows: (1) metal artifacts were more serious on the tail of the clip than those on the head on both conventional CTA and VMIs; (2) VMIs can significantly reduce metal artifacts compared with conventional CTA except for 60 keV, whether at the head, tail or middle part of the clip; (3) metal artifacts of clips near the skull base were higher than those away from the skull base on both conventional CTA and VMIs; (4) the 70–80 keV VMIs showed the best compromise between clip artifact reduction and contrast vessel visibility.

There are many causes of the artifacts of implanted metal clips, including beam hardening, photon starvation, scattering, noise, and non-linear distribution effects, mainly characterized by the appearance of light and dark stripes around the clip.[16-18] In this study, we found that there were different numbers and lengths of dark stripes in the head and tail of the clip, and the dark stripes in the tail were more serious than those in the head. The ΔCT_B value of the tail was larger than the ΔCT_A value of the head in both conventional CTA and VMIs. This may be related to the shape and position of the metal clip after implantation. The aneurysm clip is scissor-like; the shape of the head is quasi-round or similar to the number "8," and the tail is thin and long after clipping, resulting in the tail absorbing more low-energy X-ray photons and, hence, a more obvious beam hardening effect. It is characterized by a wider range of low-density dark stripes. In addition, we found that there are multiple scattered patchy or coronal high-density artifacts around the middle part of the metal clip, which may be related to noise, photon

Table 4. AI_D, AI_E, CRN_D, and CNR_E in the five groups of VMIs compared with conventional CTA

Group	AI_D (HU)	*P* value	AI_E (HU)	*P* value	CNR_D	*P* value	CNR_E	*P* value
Conventional CTA	51.94 ± 13.81	-	67.94 ± 29.52	-	5.70 ± 1.06	-	9.62 ± 4.89	-
60 keV	57.41 ± 15.59	0.007	56.50 ± 19.02	<0.001	5.92 ± 1.19	0.313	11.64 ± 4.39	0.008
70 keV	42.94 ± 11.40	<0.001	44.51 ± 14.58	<0.001	5.94 ± 1.17	0.271	11.03 ± 4.34	0.061
80 keV	32.47 ± 9.09	<0.001	37.06 ± 12.56	<0.001	5.98 ± 1.22	0.195	10.34 ± 4.14	0.336
90 keV	25.56 ± 7.09	<0.001	33.09 ± 12.21	<0.001	5.84 ± 1.20	0.527	9.27 ± 3.60	0.646
100 keV	21.20 ± 6.05	<0.001	29.88 ± 12.14	<0.001	6.72 ± 1.20	0.957	8.47 ± 3.19	0.128

VMI, virtual monoenergetic imaging; CTA, computed tomography angiography; HU, hounsfield unit.

starvation, and similar effects. It affects the observation of the brain parenchyma around the clip and may cause false positives of cerebral hemorrhage, overestimates of the extent of cerebral hemorrhage, or coverage of cerebral infarction or subarachnoid hemorrhage, resulting in misdiagnosis or missed diagnosis. Meanwhile, it also affects the observation of the vessel around the clip and interferes with the diagnosis of residual or recurrent aneurysms, vascular stenosis, or vasospasm.

X-ray tubes generate photons with different energy levels. When they encounter metal clips with high attenuation coefficients, more low-energy photons are absorbed, whereas high-energy photons penetrate. This unequal proportion of absorption characteristics causes beam-hardening artifacts and reduces image quality. The ideal way to eliminate this artifact is for the tube to output photons of the same energy; however, such a device cannot be manufactured with current technology. Dual-energy CT virtually calculates the attenuation value of each voxel at different keV levels through high-energy and low-energy scanning modes, thus generating VMIs. In this retrospective study, we researched the ability of VMI to reduce metal artifacts and enhance vascular contrast. We found that VMI can significantly reduce the metal artifacts compared with conventional CTA. The quantitative analysis showed that the ΔCT and AI at the head, tail, or middle part of the clip decreased significantly on VMIs except for 60 keV, meaning significant MAR. These results were similar to the qualitative analysis, showing a significant improvement in the proportions of brain parenchyma score ≥4 in 70, 80, and 90 keV. Several studies over the past decade[8-12] investigated the values of DECT-based VMI or MAR algorithms to reduce artifacts in clipped or coiled aneurysms. As previously mentioned, a skull phantom study[10] showed that VMI significantly reduced metal artifacts compared with non-corrected images, which was similar to our results, and performed better when combined with the iterative MAR algorithm. MAR algorithms were designed to reduce artifacts caused by metal implants at low energy while preserving good image quality. Bier et al.[8] found that iterative MAR algorithms improved non-enhanced CT image quality after clipping or coiling but did not improve single-energy CTA image quality and reduced adjacent vessel contrast in 30% of cases. They supposed that this was caused by novel artifacts generated by the over-correction of the algorithm. Furthermore, the competing interests of high-energy and low-energy images are a limitation of DECTA-based VMI. Thus, we thought that they were complementary, and a few studies have proved this.[10,11] Furthermore, MAR algorithms are available for both single-energy and dual-energy CT acquisition, whereas VMI requires a dual-energy CT scanner, which can be expensive.

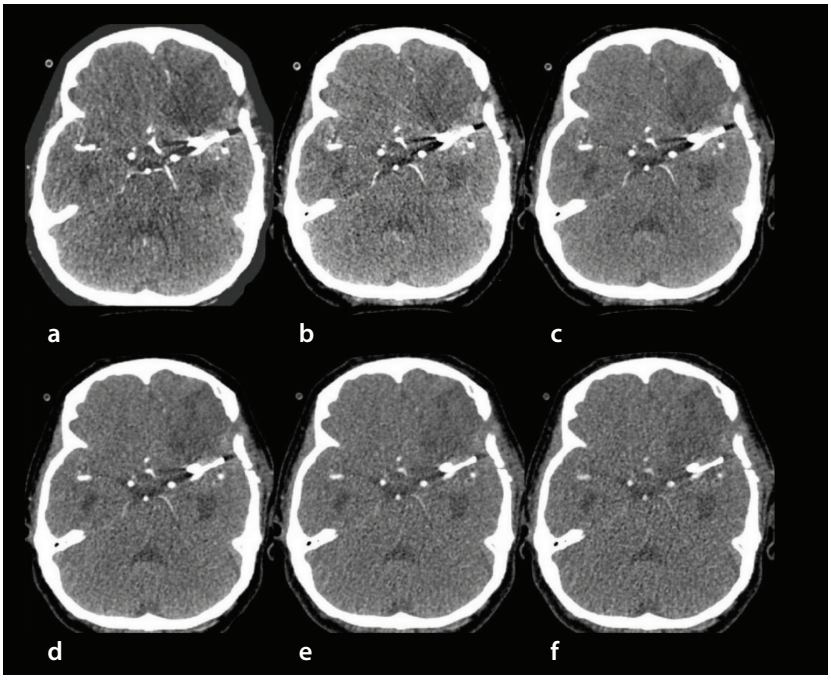

Figure 5. A 61-year-old woman underwent surgical clipping for a left middle cerebral artery aneurysm. Axial reformatted of a blended 115 kV image **(a)** and virtual monoenergetic imaging at 60 **(b)**, 70 **(c)**, 80 **(d)**, 90 **(e)**, and 100 keV **(f)** are shown. Virtual monoenergetic imaging at 70 **(c)** and 80 keV **(d)** shows the best compromise between the reduction of artifacts and contrast vessel visibility.

Table 5. Results from the qualitative analysis in the five groups of VMIs compared with conventional CTA

Group (n, %) \ Points		1	2	3	4	5	≥4	χ^2	*P* value
Brain parenchyma score	Conventional CTA	0 (0)	3 (5)	53 (88.33)	4 (6.67)	0 (0)	4 (6.67)	-	-
	60 keV	0 (0)	6 (10)	50 (83.3)	4 (6.67)	0 (0)	4 (6.67)	0.00	1.000
	70 keV	0 (0)	0 (0)	23 (38.33)	36 (60)	1 (1.67)	37 (61.67)	40.35	<0.001
	80 keV	0 (0)	1 (1.67)	11 (18.33)	48 (80)	0 (0)	48 (80)	65.70	<0.001
	90 keV	0 (0)	0 (0)	48 (80)	12 (20)	0 (0)	12 (20)	4.62	0.032
	100 keV	0 (0)	7 (11.67)	50 (83.3)	3 (5)	0 (0)	3 (5)	0.15	0.697
Cerebrovascular score	Conventional CTA	0 (0)	38 (63.33)	21 (35.0)	1 (1.67)	0 (0)	1 (1.67)	-	-
	60 keV	0 (0)	0 (0)	30 (50)	30 (50)	0 (0)	30 (50)	36.58	<0.001
	70 keV	0 (0)	0 (0)	3 (5)	56 (93.33)	1 (1.67)	57 (95)	104.65	<0.001
	80 keV	0 (0)	0 (0)	16 (26.67)	43 (71.67)	1 (1.67)	44 (73.3)	44.71	<0.001
	90 keV	0 (0)	2 (3.33)	50 (83.33)	8 (13.33)	0 (0)	8 (13.33)	5.89	0.015
	100 keV	0 (0)	17 (28.33)	43 (71.67)	0 (0)	0 (0)	0 (0)	1.01	0.315

VMI, virtual monoenergetic imaging; CTA, computed tomography angiography.

Due to the different methods and positions of metal clip implantation, the cerebral arteries of some patients are not necessarily affected by the artifacts of the head and tail of the clip simultaneously; therefore, we selected the vessel with the worst artifacts as ROI D. With the increase in keV level, ΔCT_D, ΔCT_E, AI_D, and AI_E gradually decreased, indicating that the vascular artifacts gradually decreased. Nevertheless, except for the CNR_E of 60 keV, there was no significant difference in CNR_D and CNR_E between VMIs and conventional CTA, indicating no significant increase in vascular contrast. In qualitative analysis, the proportions of cerebrovascular score ≥4 in VMIs were significantly higher than those of conventional CTA, except for 100 keV. This difference may be because CNR reflects the actual discernibility of vascular contrast in the presence of noise, whereas subjective scores evaluate the vascular contrast by comparing it with the surrounding brain parenchyma. This needs further investigation.

High-keV VMIs can reduce beam hardening artifacts,[19] a phenomenon that has also been verified in our study. However, the contrast of high-keV images decreased, and the density resolution of vessels and brain parenchyma diminished. Our results showed that the ΔCT and AI values of 90 and 100 keV were lower than those of 70 and 80 keV, but the proportions of brain parenchyma and cerebrovascular scores ≥4 were also significantly lower than those of 70 and 80 keV. The proportions of brain parenchyma and cerebrovascular scores ≥4 of 70 keV were 61.67% and 95%, respectively, and the proportions of 80 keV were 80% and 73.3%, respectively, which were higher than those of conventional CTA, 60 keV, 90 keV, and 100 keV. Therefore, we believe that 70–80 keV is the optimal energy range for evaluation after cerebral aneurysm clipping. Dunet et al.[11] reported that the best compromise between MAR and relative CNR was obtained at 70–75 keV for GSI DECTA, but they did not compare their results with conventional CTA as we did, and the relative CNRs of the contralateral middle cerebral artery and internal carotid artery far from the clip were not representative of the visibility of the vessels adjacent to the clip. In addition, we found that metal artifacts of clips near the skull base were higher than those away from the skull base, whereas their results showed that the clips' location and number did not influence the ability of GSI with or without MAR to reduce metal artifacts. This problem needs further study.

There were several limitations in our study. First, due to the relatively small patient cohort, there is no classification of different materials and sizes of clips; for example, cobalt alloy clips are known to produce more artifacts than titanium clips.[20] In addition, we only consider the patients treated by one clip, whereas it seems obvious that metal artifacts increase with the number of clips. Therefore, it is necessary to increase the sample size to further study the application value of the DECTA-based VMI technique for clips of different materials, sizes, and numbers. Second, this study is retrospective, so blended 115 kV images were used instead of conventional CTA. There may be some differences between them, although previous studies have reported that blended images are similar to conventional CT.[21] In addition, it is unethical to perform two CTA scans (single-energy and dual-energy) in the same patient. Finally, we did not compare the VMI with other MAR techniques.

In conclusion, our research demonstrated that for patients who underwent DECTA after cerebral aneurysm clipping, the 70–80 keV VMIs are expected to be the optimal energy range for balancing metal artifacts and cerebrovascular visibility. The clip artifacts of 70 keV images are lower than those of conventional CTA, and the cerebrovascular contrast can meet the clinical evaluation. Images at 80 keV can further reduce clip artifacts and better show the changes in the surrounding brain parenchyma. We recommend using them together.

Footnotes

Conflict of interest disclosure

The authors declared no conflicts of interest.

Funding

This work was supported by the Fujian Provincial Science and Technology Department, Fujian, China (grant number 2023J011727), and the Putian University, Fujian, China (grant number 2022107).

References

1. Texakalidis P, Sweid A, Mouchtouris N, et al. Aneurysm formation, growth, and rupture: the biology and physics of cerebral aneurysms. *World Neurosurg.* 2019;130:277-284. [CrossRef]
2. Cianfoni A, Pravatà E, De Blasi R, Tschuor CS, Bonaldi G. Clinical presentation of cerebral aneurysms. *Eur J Radiol.* 2013;82(10):1618-1622. [CrossRef]
3. Abla AA, Lawton MT. Predictors of complications with unruptured middle cerebral artery aneurysm clipping in a surgically treated series of 416 patients: a clip first approach is still best. *World Neurosurg.* 2015;84(4):884-885. [CrossRef]
4. Brown MA, Parish J, Guandique CF, et al. A long-term study of durability and risk factors for aneurysm recurrence after microsurgical clip ligation. *J Neurosurg*. 2017;126(3):819-824. [CrossRef]
5. Piao J, Luan T, Qu L, Yu J. Intracranial post-clipping residual or recurrent aneurysms: current status and treatment options (Review). *Med Int (Lond).* 2021;1(1):1. [CrossRef]
6. Yu LB, Fang ZJ, Yang XJ, Zhang D. Management of residual and recurrent aneurysms after clipping or coiling: clinical characteristics, treatments, and follow-up outcomes. *World Neurosurg.* 2019;122:838-846. [CrossRef]
7. Zachenhofer I, Cejna M, Schuster A, Donat M, Roessler K. Image quality and artifact generation post-cerebral aneurysm clipping using a 64-row multislice computer tomography angiography (MSCTA) technology: a retrospective study and review of the literature. *Clin Neurol Neurosurg.* 2010;112(5):386-391. [CrossRef]
8. Bier G, Bongers MN, Hempel JM, et al. Follow-up CT and CT angiography after intracranial aneurysm clipping and coiling-improved image quality by iterative metal artifact reduction. *Neuroradiology.* 2017;59(7):649-654. [CrossRef]
9. Pan YN, Chen G, Li AJ, et al. Reduction of metallic artifacts of the post-treatment intracranial aneurysms: effects of single energy metal artifact reduction algorithm. *Clin Neuroradiol.* 2019;29(2):277-284. [CrossRef]
10. Winklhofer S, Hinzpeter R, Stocker D, et al. Combining monoenergetic extrapolations from dual-energy CT with iterative reconstructions: reduction of coil and clip artifacts from intracranial aneurysm therapy. *Neuroradiology.* 2018;60(3):281-291. [CrossRef]
11. Dunet V, Bernasconi M, Hajdu SD, Meuli RA, Daniel RT, Zerlauth JB. Impact of metal artifact reduction software on image quality of gemstone spectral imaging dual-energy cerebral CT angiography after intracranial aneurysm clipping. *Neuroradiology.* 2017;59(9):845-852. [CrossRef]
12. Mocanu I, Van Wettere M, Absil J, Bruneau M, Lubicz B, Sadeghi N. Value of dual-energy CT angiography in patients with treated intracranial aneurysms. *Neuroradiology.* 2018;60(12):1287-1295. [CrossRef]
13. Waaijer A, Prokop M, Velthuis BK, Bakker CJ, de Kort GA, van Leeuwen MS. Circle of Willis at CT angiography: dose reduction and image quality--reducing tube voltage and increasing tube current settings. *Radiology.* 2007;242(3):832-839. [CrossRef]
14. Christner JA, Kofler JM, McCollough CH. Estimating effective dose for CT using

dose-length product compared with using organ doses: consequences of adopting International Commission on Radiological Protection publication 103 or dual-energy scanning. *AJR Am J Roentgenol.* 2010;194(4):881-889. [CrossRef]

15. Yun SY, Heo YJ, Jeong HW, et al. Dual-energy CT angiography-derived virtual non-contrast images for follow-up of patients with surgically clipped aneurysms: a retrospective study. *Neuroradiology.* 2019;61(7):747-755. [CrossRef]
16. Bucher AM, Wichmann JL, Schoepf UJ, et al. Quantitative evaluation of beam-hardening artefact correction in dual-energy CT myocardial perfusion imaging. *Eur Radiol.* 2016;26(9):3215-3222. [CrossRef]
17. Wellenberg RHH, Hakvoort ET, Slump CH, Boomsma MF, Maas M, Streekstra GJ. Metal artifact reduction techniques in musculoskeletal CT-imaging. *Eur J Radiol.* 2018;107:60-69. [CrossRef]
18. Mori I, Machida Y, Osanai M, Iinuma K. Photon starvation artifacts of X-ray CT: their true cause and a solution. *Radiol Phys Technol.* 2013;6(1):130-141. [CrossRef]
19. Katsura M, Sato J, Akahane M, Kunimatsu A, Abe O. Current and novel techniques for metal artifact reduction at CT: practical guide for radiologists. *Radiographics.* 2018;38(2):450-461. [CrossRef]
20. van der Schaaf I, van Leeuwen M, Vlassenbroek A, Velthuis B. Minimizing clip artifacts in multi CT angiography of clipped patients. *AJNR Am J Neuroradiol.* 2006;27(1):60-66. [CrossRef]
21. Marin D, Boll DT, Mileto A, Nelson RC. State of the art: dual-energy CT of the abdomen. *Radiology.* 2014;271(2):327-342. [CrossRef]

Supplementary Table S1. Five-point Likert scale for evaluation of the artifacts severity of brain parenchyma and the cerebrovascular visibility

Points	Brain parenchyma score	Cerebrovascular score
1	Severe artifacts, mostly not diagnostic	Severe artifacts, mostly not diagnostic
2	Poor image quality, partly non-diagnostic	Reduced vessel delineation, partly non-diagnostic
3	Moderate image quality, limitedly diagnostic	Partly limited vessel contrast, limitedly diagnostic
4	Good image quality, enough for diagnostic	Good vessel delineation, enough for diagnostic
5	Perfect image quality, no artifacts	Excellent vessel delineation, no artifacts

Supplementary Table S2. Details of clips used in the study

No.	Model	Material	Blade length (mm)	Shape	Maximum opening (mm)	Closing force (N)	Closing force (g)	Specification
1	FT740T	Titanium	7.0	Straight	6.2	1.47	150	Yasargil, Braun Medical, Tuttlingen, Germany
2	FT742T	Titanium	6.5	Curved	6.0	1.47	150	Yasargil, Braun Medical, Tuttlingen, Germany
3	FT750T	Titanium	9.0	Straight	7.0	1.77	180	Yasargil, Braun Medical, Tuttlingen, Germany
4	FT752T	Titanium	8.3	Curved	6.8	1.77	180	Yasargil, Braun Medical, Tuttlingen, Germany
5	FT760T	Titanium	11.0	Straight	7.8	1.77	180	Yasargil, Braun Medical, Tuttlingen, Germany
6	FT762T	Titanium	10.2	Curved	7.5	1.77	180	Yasargil, Braun Medical, Tuttlingen, Germany
7	FT782T	Titanium	13.7	Curved	8.7	1.96	200	Yasargil, Braun Medical, Tuttlingen, Germany

Supplementary Table S3. Study patients' characteristics (n = 60)

Characteristics	Mean ± SD or n
Age (years)	55.15 ± 9.24
Male/female	23/37
Aneurysm localization (left/right)	
Anterior communicating artery	17
Anterior cerebral artery	2/1
Middle cerebral artery	17/6
Posterior cerebral artery	1/0
Internal carotid artery	8/6
Posterior communicating artery	0/2
Postoperative complication	
None	9
Cerebral hemorrhage	20
Cerebral infarction	7
Encephaledema	33
Hydrocephalus	12
Epidural or subdural hematoma	20
Subarachnoid hemorrhage	12
Cerebral vasospasm	8
Residual aneurysm	2

SD, standard deviation.

Supplementary Table S4. Inter-reader and Intra-reader ICCs regarding attenuation and SD values of ROIs in the six groups of images

Parameters		Conventional CTA	60 keV	70 keV	80 keV	90 keV	100 keV
Attenuation	ROI A	0.901/0.912	0.953/0.924	0.940/0.936	0.921/**0.995**	0.981/0.981	0.978/0.946
	ROI B	0.893/0.951	0.898/0.979	0.972/0.970	0.982/0.931	0.940/0.944	0.937/0.945
	ROI C	0.906/0.956	0.921/0.945	0.907/0.952	0.971/0.967	0.977/0.916	0.934/0.930
	ROI D	0.926/0.945	0.936/0.992	0.923/0.957	0.960/0.943	0.923/0.920	0.942/0.925
	ROI E	0.967/0.934	0.935/0.929	0.898/0.925	0.965/0.918	0.956/**0.995**	0.936/**0.911**
	OLP	0.925/0.937	0.977/0.935	0.943/**0.911**	0.950/0.955	0.956/0.970	0.902/0.969
	BA	0.907/0.990	0.907/0.981	0.923/0.937	0.934/0.942	0.914/0.990	**0.892**/0.913
SD	ROI A	0.907/0.953	0.949/0.937	0.923/0.974	0.938/0.957	0.934/0.985	0.911/0.929
	ROI B	0.932/0.947	0.906/0.967	0.981/0.953	0.937/0.918	0.975/0.918	**0.892**/0.965
	ROI C	0.899/0.990	0.954/0.927	0.959/0.988	0.963/0.923	0.931/0.945	0.901/0.940
	ROI D	0.948/0.918	0.909/0.976	0.907/0.961	0.940/0.939	0.904/0.985	0.942/0.978
	ROI E	0.972/0.924	0.934/0.972	0.953/0.945	0.939/0.955	0.923/0.930	0.953/0.957
	OLP	0.912/0.916	0.972/0.972	0.928/0.989	0.955/0.940	**0.985**/0.929	0.926/0.960
	BA	0.974/0.966	0.928/0.977	0.928/0.929	0.943/0.982	0.971/0.986	0.980/0.980

Please note that these values were inter-reader ICC/intra-reader ICC. ROI, region of interest; CTA, computed tomography angiography; SD, standard deviation; OLP, occipital lobe parenchyma; BA, basilar artery; ICC, intraclass correlation coefficient.

Supplementary Table S5. Comparison of the severity of metal artifacts between clips near or away from the skull base in the six groups of images

	ΔCT_{near} (HU)	ΔCT_{away} (HU)	Z	*P*	AI_{near} (HU)	AI_{away} (HU)	Z	*P*
Conventional CTA	288.51 ± 103.21	208.27 ± 80.27	-3.252	0.001	93.80 ± 49.66	62.63 ± 42.24	-2.756	0.006
60 keV	347.88 ± 115.83	249.64 ± 101.54	-3.252	0.001	104.76 ± 57.39	71.25 ± 48.83	-2.483	0.013
70 keV	239.27 ± 79.55	168.64 ± 66.31	-3.397	0.001	73.76 ± 39.62	51.07 ± 33.50	-2.451	0.014
80 keV	164.50 ± 59.43	119.28 ± 45.45	-2.804	0.005	53.54 ± 28.80	38.70 ± 23.04	-2.163	0.031
90 keV	112.42 ± 45.83	81.81 ± 29.60	-2.980	0.003	39.23 ± 22.11	30.16 ± 16.55	-1.730	**0.084**
100 keV	74.92 ± 37.98	56.27 ± 21.32	-2.451	0.014	30.82 ± 18.67	25.83 ± 13.47	-0.961	**0.336**

ΔCT_{near}, ΔCT of clips near the skull base; ΔCT_{away}, ΔCT of clips away from the skull base; AI_{near}, artifact index of clips near the skull base; AI_{away}, artifact index of clips away from the skull base; Z/*P*, statistics/significance of Mann-Whitney U test; HU, hounsfield unit; CTA, computed tomography angiography.

Supplementary Table S6. Cohen's kappa coefficients of the scores between radiologists 1 and 2 in the six groups of images

Score	Conventional CTA	60 keV	70 keV	80 keV	90 keV	100 keV
Brain parenchyma score	0.633	0.771	0.666	0.725	0.832	0.691
Cerebrovascular score	0.797	0.694	0.706	0.691	0.694	0.697

CTA, computed tomography angiography.